

Deep Learning-Based CT Radiomics for Feature Representation and Analysis of Aging Characteristics of Asian Bony Orbit

Zhu Li, PhD,* Kunjian Chen, MS,* Jiayu Yang, MS,* Lei Pan, MD,† Zhen Wang, MD,‡ Panfeng Yang, MD,‡ Sufan Wu, PhD, MD,† and Jingyu Li, PhD†

Objective: This paper puts forward a new method for automatic segmentation of bony orbit as well as automatic extraction and classification of aging features of segmented orbit contour based on depth learning, with which the aging mode of bony orbit contour is preliminarily validated.

Method: Three-dimensional reconstruction was carried out by using the craniofacial Computed Tomography scanning data of 595 adult Mongolians at different ages (119 young males, 78 young females, 109 middle-aged males, 89 middle-aged females, 95 elderly males, and 105 elderly females), the craniofacial images were exported, orbit contour images were obtained with U-Net segmentation network, and then the orbit contour features of young group, the middle-aged group and the elderly group were classified with the classification network. Next, contour area, height, and other features put forward in existing research were automatically calculated by using the connected component shape description method; and it was validated whether the aging features of the bony orbit only occur to partial or the whole orbit.

Results: With the method put forward in this paper, high-precision identification (97.94% and 99.18%) of 3 categories in the male and

female group experiments. In the meanwhile, it was found in the comparison experiment with other features that bony orbit contour definitely has features relating to aging, but these features only occur to partial areas of the orbit, which enables the convolutional neural network to achieve good identification effects. And, bone resorption of the superior orbital rim of males is more obvious than that of the inferior orbital rim, but the overall shape features like the bony orbit area and height do not change significantly along with the increase of the age.

Conclusions: U-Net can realize high-precision segmentation of the orbit contour, and with the Convolutional Neural Network-based orbit contour sorting algorithm, the aging degree of the bony orbit can be identified precisely. It is preliminarily validated that the aging mode of Mongolian bony orbit contour is that the bone resorption of the superior orbital rim is more obvious than that of the inferior orbital rim, and the change of the orbit area, perimeter, height and circularity is not obvious in the aging process.

Key Words: Aging characteristic, bony orbit, CT, deep learning, radiomics

(*J Craniofac Surg* 2022;33: 312–318)

From the *School of Electronics and Information, Hangzhou Dianzi University; †Department of Plastic and Reconstructive Surgery; and ‡Department of Radiology, People's Hospital of Hangzhou Medical College, Zhejiang Provincial People's Hospital, Hangzhou, China.

Received May 10, 2021.

Accepted for publication August 24, 2021.

Address correspondence and reprint requests to Lei Pan, MD, and Zhen Wang, MD, People's Hospital of Hangzhou Medical College, Zhejiang Provincial People's Hospital, 158# Shangtang Road, Hangzhou 310014, China; E-mail: prs_dr_panlei@163.com, wang12345zhen@sina.com

ZL and KC are the co-first authors.

This work was supported by the General Project Funds from the Health Department of Zhejiang Province (Grant No. 2019324435), the General Project Funds from the Health Department of Zhejiang Province (Grant No. 2021KY480), and the Public Welfare Technology Research Program of Zhejiang Province China (No. LGF21H150004).

The authors report no conflicts of interest.

Supplemental digital contents are available for this article. Direct URL citations appear in the printed text and are provided in the HTML and PDF versions of this article on the journal's Web site (www.jcraniofacialsurgery.com).

This is an open access article distributed under the terms of the Creative Commons Attribution-Non Commercial-No Derivatives License 4.0 (CCBY-NC-ND), where it is permissible to download and share the work provided it is properly cited. The work cannot be changed in any way or used commercially without permission from the journal.

Copyright © 2021 The Author(s). Published by Wolters Kluwer Health, Inc. on behalf of Mutaz B. Habal, MD.

ISSN: 1049-2275

DOI: 10.1097/SCS.000000000000198

As the age increases, people's facial bones,¹ skin,² and various soft tissues³ will change constantly, consequently the face will present aging characteristics, its changing rules are of great research value⁴ in the field of cosmetic plastic surgery. Facial bone as a facial support, whose change may have a knock-on effect on other facial tissues, so bone morphology is an important branch of researches on face aging.^{5–7} Computed Tomography (CT)-based radiomics is widely used for study of aging characteristics. According to Lambros theory,⁸ as people grow older, the maxilla displaces posteriorly, inferior orbital rim laterally moves and the lower jaw contract in vertical and horizontal planes. Mendelson et al⁹ recorded the length of the orbital roof and orbital floor for each patient, along with the angle between the orbital floor and the anterior wall of the maxilla using facial CT images. They found that with the increase of age, the changes in different parts of the facial bone were uneven and the angle between the anterior wall of maxillary and the orbital floor decreased with age, which was also confirmed in the research of Shaw and Kahn¹⁰ Sung et al¹¹ found that the canine fossa would become more sunken with age for both men and women, and they believed this change can be regarded as 1 of the signs of facial bones aging.

The morphological change in bony orbit during senescence is also a hot topic of study.^{12–14} Wherein, Kahn and Shaw¹⁵ reconstructed the craniofacial CT data and then created a horizontal line from the intersection of the lateral orbital rim and frontozygomatic suture to the posterior lacrimal crest of the three-dimensional (3D)

model. The line was equal in length to the orbital aperture width, and was equally divided into 10 parts, and the vertical distance from each point to the supraorbital and the inferior orbital rim was measured manually. Through the study on the craniofacial features of 60 American people (30 for female and male, respectively), they found that the bony orbit gradually expanded with age, and the orbital area of males was larger than that of females in all age groups. And they also found that the orbital aperture width for both genders increased with age. Unlike Pessa’s findings,¹⁶ Pessa’s study on 30 male skulls showed no significant change with age in above-mentioned aspects. Kahn and Shawjr¹⁵ also found that bone resorption occurred in the medial side of both male and female supraorbital margin with the increase of age, but in the whole inferior orbital rim in male, whereas only in the lateral side of inferior orbital rim in female. On the contrary, Pessa and Chen¹⁶ considered that the inferior orbital rim had fewer areas of bone resorption, and that there were significant changes only in middle and old age. Ching et al¹⁷ statistically analyzed the left and right orbital volume, vertical height, orbital aperture width, length of bilateral orbital wall, length of superior, and inferior orbital rim in 70 patients (35 for each gender) of 7 age groups. The analysis showed that the orbital volume of both genders was not associated with age, however, the orbital volume of males was larger than that of females. It was also found that the lateral orbital wall lengthened with age, but the vertical height of the orbit and the orbital aperture width had nothing to do with the age. Jeon et al¹⁸ took the most lateral, medial, superior, and inferior points of orbital rim as reference points to analyze the bony orbital height and area of 107 Koreans (52 females and 55 males) on the craniofacial 3D model, whose results suggested that the height and area did not increase significantly with age, which was different from the results of Kahn.¹⁵

To sum up, some achievements have been made in the present research on the relationship between bony orbital characteristics and senescence, however, there are some contradictory conclusions primarily resulting from few experimental samples in the current studies, with only dozens of men and women, respectively, on the 1 hand, the collection of experimental samples is not an easy thing, and on the other hand, the measurement of orbital characteristics for each subject is necessarily measured manually by professionals, therefore, the efficiency is not high, and it is difficult to test large datasets swiftly.

In recent years, deep learning plays an increasingly significant role in the field of medical image processing. Like in the field of lesion detection, the identification of coronavirus disease 2019 patients,¹⁹ the establishment of a cervical cancer screening system,²⁰ and the identification of patients with blowout fracture of orbit,²¹ etc. utilize this technology. In this paper, it is first necessary to segment the craniofacial image to obtain the orbital contour. U-Net proposed by Ronneberger et al²² is 1 of the most effective segmentation algorithms based on deep learning. It can achieve accurate pixel-level segmentation with less data, and typically rapidly collecting large amounts of samples is a difficult medical task. Thus, U-Net is widely applied in the field of medical image segmentation, such as the segmentation of ultrasound mammary mass,²³ the segmentation of glioma,²⁴ and the division of nucleus,²⁵ etc.

METHODS

In this paper, deep learning is used to realize the automatic segmentation of bony orbit and the automatic feature representation and classification of orbital aging features based on the segmentation results. The main content is as shown below:

- (1) This paper presents a 3-category recognition method based on CT radiomics for youth, middle-aged, and elderly. The orbital contour images are obtained through U-Net, then the images are classified through convolution neural network so as to finally get final recognition results, the accuracy rate is over 97%.

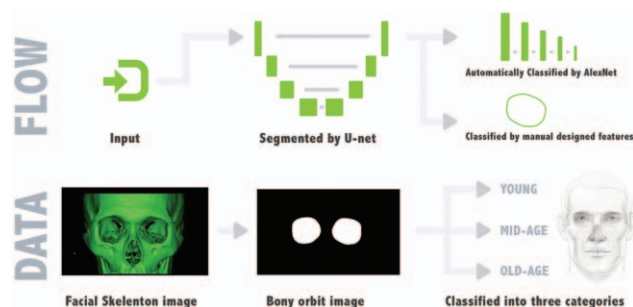


FIGURE 1. Method flowchart.

- (2) In this paper, an automatic feature representation method of bony orbital contour is put forward, which can automatically extract partial features of orbital contours. This method is used to verify the correlation of the orbital characteristics, including its area and height with aging, which has been raised in previous studies.
- (3) In this paper, the recognition experiments are carried out through the convolution neural network, shape context and shape features of the connected component, and the aging pattern of the bony orbit is initially proven depending on the contrast of the recognition results.
- (4) All the codes used in this paper have been open-sourced¹. In order to perfect the study of the relationship between bony orbit and senescence, medical workers can use the method proposed in this paper to study and verify swiftly on larger datasets.

In this research, the craniofacial image dataset was prepared first, and then the image segmentation network U-Net was used to obtain the orbit contour images, the convolutional neural network (hereinafter referred to as “CNN”) was used to carry out automatic extraction and classification of features, and the automatic orbit shape feature extraction method was used to classify and validate the orbit area and other many features. The method process is as shown in Figure 1 “FLOW.” Data processed in each stage of the method are as shown in Figure 1 “DATA.”

Image Segmentation Network Preparation of Cranial Image

Three-dimensional reconstruction of skull CT scanning data in Digital Imaging and Communications in Medicine format is carried out using Mimics 21.0 (Materialise, Leuven, Belgium), and the facial bone is adjusted to the standard front view with the same method as the literature.²⁶ Details can be found in the literature.²⁶ And in the following, a 70-mm line segment in the software space as a ruler, and then the craniofacial elevation view is derived, afterwards the ruler is used to scale the image so that its ratio to the real distance is 27.333 pixels per centimeter, and finally the size of each image is adjusted to 600*360, as shown in Figure 2A.

Image Segmentation

After craniofacial elevation view is obtained, U-Net is used to segment the image in order to get the orbital contour image in this paper. The first step of the segmentation is to annotate the training data. The original image and the corresponding annotated image are shown in Figure 2. The basis for determining the bony orbital rim in the annotating: select the lateral border of orbital rim shadow. If the supraorbital foramen is not fused with the superior orbital rim, the

¹ <https://github.com/lizhu1126/Aging-of-the-Bony-Orbit>.

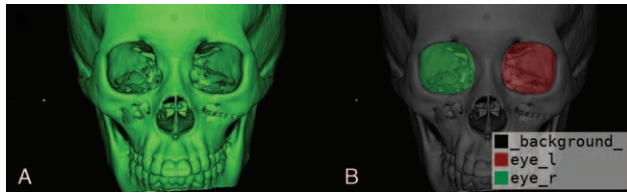


FIGURE 2. Craniofacial image and its annotated image. (A) A craniofacial image. (B) The annotation image.

course of superior orbital contour should be followed. If the 2 are fused, the outline of the supraorbital margin is determined by the superior margin of the supraorbital foramen.

The network architecture of U-Net is shown in Figure 3. The overall architecture consists of 2 components: a contracting path (left side) and an expansive path (right side). The former is used to capture contextual information and the latter is used to pinpoint the target. The contracting path is composed of 2 repeated applications of convolution with a convolution kernel 3*3. Each convolution is followed by a rectified linear unit (ReLU) and a max-pooling layer with a size of 2*2. Followed by 4 consecutive down sampling, the resolution of the feature map progressively decreases and the number of channels come to increases. The expansive path adopts the upper sampling layer of 2*2 to halve the number of characteristic channels, then it is concatenated with the corresponding cut feature map from the contracting path, and then 2 convolutions of 3*3 are done, which is followed by a ReLU activation function for each. At the last layer, 1*1 convolution is used to map each sixty-four-dimensional feature vector to the desired number of classes. According to the self-made dataset, the input of U-Net network modified to 600*360, and the output is of 2 types in this paper.

**Feature Description Method
Convolutional Neural Network**

In the segmented orbital images, left and right eyes are marked in different colors and cut to 360*360 in size, as shown in Figure 4A. It is not necessary to use convolution neural network with too many layers for feature extraction, given few characteristics included in orbital contour images without complex changes in color. If the structure of the identification model is excessively deep, it will lead to problems such as over-fitting and increasing calculation. Thus, in this paper, modifications are made on the basis of AlexNet²⁷ and then a classification network is constructed.

The network structure is shown in Figure 5. The network consists of 5 convolution layers and 3 connected layers. The first 2 convolution layers and the fifth convolution layer follow a max-pooling layer, and the first 7 layers adopt the ReLU activation

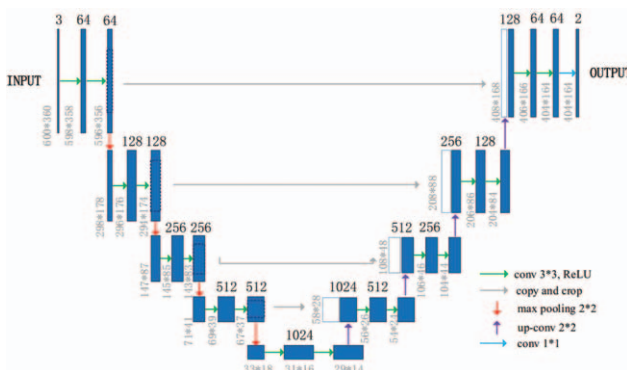


FIGURE 3. U-Net network structure.

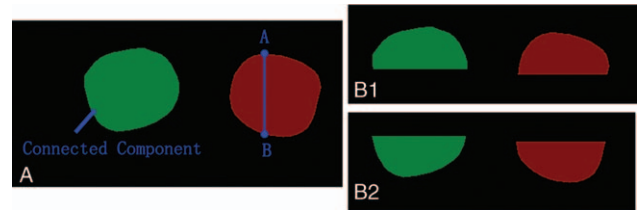


FIGURE 4. Images of complete orbital contour and upper and lower orbital images. (A) A orbital contour image. (B1-B2) Two parts of the orbital contour image.

function. In addition, the dropout²⁸ mechanism is added in the training process, and the mechanism randomly deletes a half size subset of neurons in each forward and back propagation of the training network, which can reduce the interaction between hidden neurons, thus prevent the over-fitting phenomenon so that the trained network will have more accurate results. According to the dataset used in this paper, the network input image is modified to 360*360, so as to output 3 categories: the young, middle-aged and elderly.

Description Method of Connected Component Shape

In order to determine whether the area^{15,16,18} and height^{17,18} of bony orbit change with age, the characteristics of the orbit are extracted and analyzed automatically by means of connected component shape descriptor in this paper. The connected component refers to the collection region of adjacent pixels composed of the same pixel value in the image. For example, there are 2 connected domains, that is, left and right orbital regions, as shown in Figure 4A. In addition, the relationship between orbital shape and age is analyzed by the perimeter and roundness of bony orbit. As shown in Figure 4A, point A is the highest point of the supraorbital margin and point B is the point at which the vertical line passing through point A intersects the infraorbital margin. The true length of segment AB equals to the height of the bony orbit. Roundness C_r is the degree to which a connected component is shaped close to a circle and is defined as follows:

$$C_r = \frac{F}{\pi * MD^2} \tag{1}$$

Wherein, F is the area of the connected component and MD is the maximum distance from the center of the connected component to its boundary.

Shape Context Method

In order to further determine whether the aging characteristics of the bony orbit profile exist in the whole or local area of the orbital contour, the shape context algorithm is adopted to classify the orbit of different age groups in this paper. The shape context algorithm^{29,30} treats the contours of the image as a set of points to match the point set, so that the similarity between contours is

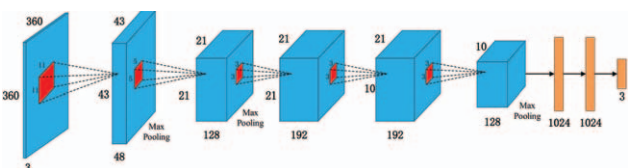


FIGURE 5. Classification network structure.

measured by the calculating similarity, and then the contours are classified and recognized.

The difference between the 2 object shapes is measured by the shape context distance which name is D_{SC} , and the smaller D_{SC} indicates more similarities between the 2 shapes. The 2 orbital contours with high similarity are determined to belong to the same age group.

Experiment

The dataset used for validation in this article is from Zhejiang Provincial People's Hospital, China. CT data of 595 cases at different ages are included. There are both males and females who are divided into 3 groups: young cases (at the age of 18–39), middle-aged cases (at the age of 40–59) and elderly cases (at the age ≥ 60). The age distribution is as shown in Supplementary Digital Content, Table 1, <http://links.lww.com/SCS/D344>. In this paper, the method was validated with the Pytorch platform and the Opencv4.4.0 library, and the testing was carried out in the host configured with Intel Corei9 3.7 GHz processor, 32GB memory and RTX3080 graphics card. This research has been approved by the Ethics Committee of Zhejiang Provincial People's Hospital.

U-Net Training

In the course of U-Net segmentation network training, 536 and 59 out of 595 cranial images sized 600*360 were used randomly as training sets and test sets, respectively. Root Mean Square prop as the training method used the cross-entropy loss function, the batch size was 8, iteration cycles were 200, and the initial learning rate was 0.0001. When the segmentation accuracy was not amplified for 2 consecutive cycles, the learning rate attenuated exponentially with the decay rate of 0.9. After training 200 epoches, the loss kept stable around 0.03, and the D_{SC} kept stable around 98%. After training, prediction was carried out on the testing set.

Classification Network Training

In this experiment, the dataset was self-made, all subjects were divided into young group, middle-aged group and elderly group by their age, the image was 360*360*3. This experiment adopted data enhancement techniques like adding noises in images and then the augmented dataset was divided at random into the training set, the validation set and the testing set in the proportion of 8:1:1. The 2 models by sex were trained during the process, taking Adam³¹ as the gradient descent algorithm. The cross-entropy loss function was used, the batch size was set to 8, the initial learning rate was 0.0001, and iteration cycles were 2000. The loss convergence result of males and females was around 0.4 and 0.35, respectively, and the final validation accuracy convergence result of males and females was around 99% and 95%, respectively.

In order to verify the change in bone absorption between the superior orbital rim and inferior orbital rim as the age increases,^{15,16} the complete orbit was halved into upper and lower orbital regions, as shown in Figure 4B1 and B2. Taking the male as an example, the classification and recognition experiments were carried out using CNN, and the hyperparameters were set in accordance with the experiment of whole image above.

Experiments on Shape Descriptor of Connected Component

In order to verify the relationship between connected component area and height of bony orbit and senescence, the area and height distribution in the male group of different ages were observed, the data from the same sex was then randomly divided into training set and testing set in 4:1, training set was for training K Nearest

Neighbor (KNN)³², the test set was used to test the classification accuracy of the model. Synthesize 4 features: the area, height, perimeter, and roundness of the connected component of bony orbit are used in turn to train KNN and visualize the training sample. For a test sample, KNN identifies the k training sample closest to it in the training set based on a range measurement, and then selects the most frequent categories of k training samples to be the predictive result. In this experiment, the distance is between the sample point and training sample is calculated by Euclidean distance, and the accuracy of classification when k is measured from 1 to 10 times for each k value ten times, and the accuracy of final classification is the average of the total measurements.

Shape Context Experiment

In this experiment, taking the left orbit as an example. This experiment divides the image data into a template set and a test set, and the distribution is as follows: for men, there are 23 templates and 96 tests in the youth group; 21 templates and 88 tests in the middle-aged group; 19 templates and 76 in the elderly group. For women, there are 15 templates and 63 tests in the youth group; 17 templates and 72 tests in the middle-aged group; 21 templates and 84 tests in the elderly group. Each image in the test set was matched with 3 types of templates of the same sex, and the average shape distance D_{SC} between the image and the 3 templates was calculated, and then through the comparison of the 3 calculated values, the D_{SC} with the lowest average was identified as the category in which the current matching image was located. Five-fold cross validation of this experiment was performed,³³ namely, the complete set of data was equally divided into 5 parts, 1 out of 5 was used as a template for each experiment, and the rest were used for testing, each time different test samples were used to calculate the accuracy of the classification.

RESULTS

U-Net Image Segmentation Results

In this paper, the dice similarity coefficient as the evaluation index of segmentation accuracy is used to express the similarity between the predicted results and the real values of the model. Its value ranges from 0 to 1. The higher value suggests a better result of image segmentation. The definition is as shown in formula (2), where A_M and A_P are the real value and predicted value, respectively, and $|\bullet|$ means absolute value.

$$DSC = \frac{2|A_M \cap A_P|}{|A_M| + |A_P|} \quad (2)$$

After training, for the prediction result of all the testing sets, the segmentation precision was calculated based on the dice similarity formula. The final dice similarity coefficient value was 97.55%. The U-Net segmentation result was almost the same as the manual segmentation result, indicating that the effect of segmentation of the orbit area in the craniofacial images with U-Net is good, and high-precision orbit images can be output for following classification experiments.

Classification Network Identification Results

Image classification tasks use Accuracy, Precision, Recall and F1-Score to measure the accuracy of identification. Accuracy represents the proportion of the correct prediction result in the total observed value; Precision represents the proportion of the correct results in which the model prediction is a positive example. Recall represents the proportion of the correct prediction results in the samples in which the real situation is a positive example; F1-

Score represents the harmonic average of Precision and Recall, and its values range from 0 to 1. The higher value shows more accurate output of the model. The calculation method shall be as follows:

$$\text{Accuracy} = \frac{TP + TN}{TP + TN + FP + FN} \tag{3}$$

$$\text{Precision} = \frac{TP}{TP + FP} \tag{4}$$

$$\text{Recall} = \frac{TP}{TP + FN} \tag{5}$$

$$\text{F1-Score} = \frac{2 \times \text{Precision} \times \text{Recall}}{\text{Precision} + \text{Recall}} \tag{6}$$

TP represents the number of positive samples correctly classified; FP represents the number of negative samples incorrectly identified as positive; FN represents the number of positive samples incorrectly identified as negative; TN represents the number of negative samples of negative samples correctly classified.

Supplementary Digital Content, Table 2, <http://links.lww.com/SCS/D344> show the test results of different age groups for both genders. For example, there are 54 young men, of which 52 are correctly identified as young, 2 are incorrectly identified as middle-aged, and no samples are mistakenly identified to be the elderly. According to Supplementary Digital Content, Table 2, <http://links.lww.com/SCS/D344>, 4 evaluation indicators for classification effectiveness in Supplementary Digital Content, Table 3, <http://links.lww.com/SCS/D344> can be further obtained. The analysis of Supplementary Digital Content, Table 3, <http://links.lww.com/SCS/D344> shows that the classification network has a good effect on the classification of male and female orbits, with an accuracy of 97.94% and 99.18%, respectively. This indicates that the shape of bony orbit in male and female is greatly correlated with the degree of senescence as they grow older, and the characteristics of orbital contours can be extracted via CNN to automatically classify different age groups.

Supplementary Digital Content, Table 4, <http://links.lww.com/SCS/D344> shows the testing results of the training model of the upper half part and the lower half part of males' orbits. Indexes of 2 models can be obtained through calculation (Supplementary Digital Content, Table 5, <http://links.lww.com/SCS/D344>). It is found that the testing accuracy of 2 parts was 98.13% and 84.47%, respectively. The accuracy of the upper half part was far higher than that of the lower half part. This may be because of different changes of the inferior orbital rim and the superior orbital rim along with the increase of the age. Wherein, more feature changes occur to the superior orbital rim than the inferior orbital rim as the age increases. As the age increases, the middle part of the superior orbital rim gets sunken upward continuously, that is, bone resorption of the middle part of the superior orbital rim is more obvious than that of the inferior orbital rim (Figs. 6 and 7), which verifies the view of the literature.¹⁶ Figure 8 displays the orbit and orbit contour of more samples, from all of which this phenomenon can be observed.

Classification Results by the Connected Component Shape Description

Figure 9A-B shows the automatic feature representation of bony orbit area and height in all age groups. The one-dimensional distribution of all samples is difficult to be observed, so it is

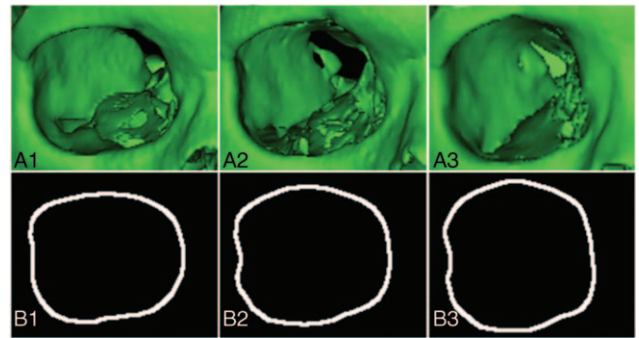


FIGURE 6. Images of the right orbit and contour of 3 samples of each age group. ([A1-B1] the young group; [A2-B2] the middle-aged group; [A3-B3] the elderly group). (A1-A3) The images of the right orbits of 3 samples picked up at random from 3 age groups. (B1-B3) The bony orbit contour images of (A1-A3). Zoom-out or zoom-in was not applied to any of them.

extended to two-dimensional image in Figure 9A-B. It can be observed that the bony orbit area in all age groups is distributed from 10 to 13 cm² and the height distribution is from 33 to 41 mm. It follows that the area and height of bony orbit are not definitely correlated with age.

In this paper, the perimeter and roundness of the orbital connected component are also used in the KNN experiment in order to further verify whether the overall contour of the bony orbit is associated with aging. In the experiment, 3 of the 4 characteristics were used 1 by 1, with 4 groups of men and women, respectively. Figure 9C-D shows the accuracy of KNN classification for different k-values under different combinations of characteristics. Group 1 is a combination of the area, height, and perimeter of bony orbit; Group 2 is the combination of its area, height, and roundness. Group 3 is the combination of its area, perimeter, and roundness. Group 4 is the combination of its height, perimeter, and roundness. We can infer that different k values have little effect on classification accuracy, and that the accuracy rate is less than 50%, regardless of any combination of 3 characteristics. Figure 9E-F shows 3D spatial mapping results of the area, height, and roundness of the bony orbit in men and women, with red, green, and blue,

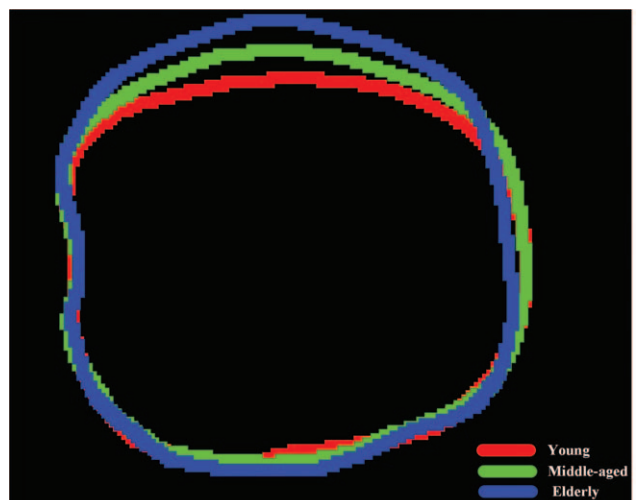


FIGURE 7. Comparison of right orbit contour images of 3 samples of each age group. (B1) to (B3) in Figure 6 were overlapped in the original proportion. Wherein, red, green and blue represent the orbit contour of young cases, middle-aged cases and elderly cases.

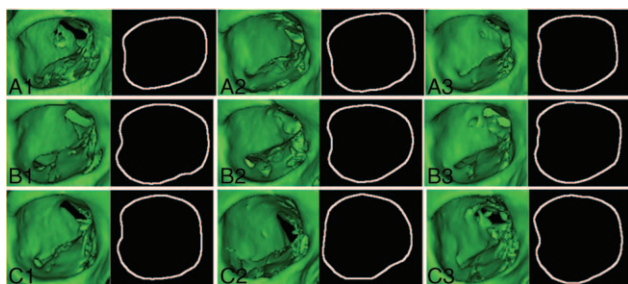


FIGURE 8. Right orbit and contour images of 3 samples of each age group ([A1-A3] young group; [B1-B3] middle-aged group; [C1-C3] elderly group).

respectively, representing the data of the young, middle-aged, and the elderly groups. It can be observed that there is no significant limit on the distribution of data among age groups, resulting in poor classification accuracy of KNN. It may be because of the large individual difference in the orbital size and so on among individuals of the same age group, which makes it impossible to classify the orbital contour images with high precision, that is, there is little correlation between the overall shape characteristics of the contours and the ageing degree of the outline in the samples.

Experiment Results on Shape Context

In order to investigate whether the aging characteristics of bony orbit is present locally or as a whole, this paper compares the experimental results of the shape context classification with the experimental results of CNN, as is shown in Supplementary Digital Content, Table 6, <http://links.lww.com/SCS/D344>. It shows that the

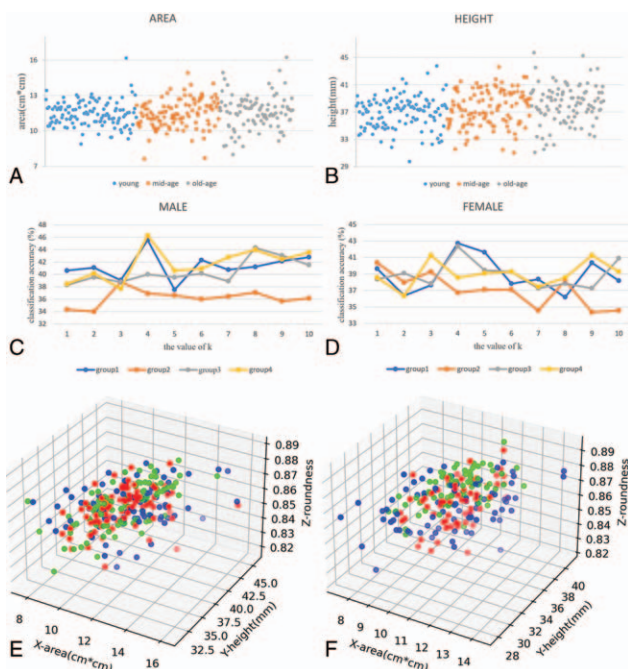


FIGURE 9. Connected component feature representation. (A) Distribution of bony orbit area for all age groups in male. (B) Distribution of bony orbit height for all age groups in male. (C) KNN classification accuracy of different k values under different feature combinations of male. (D) KNN classification accuracy of different k values under different feature combinations of female. (E) Projection of bony orbit area, height, and roundness of male in feature space. (F) Projection of bony orbit area, height, and roundness of female in feature space. KNN, K Nearest Neighbor.

accuracy of classification via the shape context algorithm is much lower than that of CNN classification. It may be because bony orbit locally varies with age, but the shape context algorithm gives the same weight to all areas of orbital contour. CNN can concentrate feature extraction in important local areas via training, so CNN is better suited for the classifying the orbital contours. In the follow-up work, CNN visualization can be used to further determine the specific relationship between every local region of orbital contour and senescence.

DISCUSSION

In this paper, the aging mode of the bony orbit was preliminarily validated through an identification experiment based on the automatic extraction algorithm of multiple features. All the research conclusions were obtained on the basis of analyzing the experimental results of the self-built dataset in this paper. Due to the privacy stipulation, we cannot disclose our dataset on the internet, but we offer open-source codes used in the experiment for further research and validation of other researchers.

In this paper, bony orbit contour images were obtained through automatic segmentation with U-Net, and then precise identification (97.94% and 99.18% for male experiment and female experiment, respectively) of Mongolian bony orbits of 3 groups (the young group, the middle-aged group, and the elderly group) was realized through automatic classification with CNN, and it was verified that bony orbit contour images actually have features strongly associated with the aging degree. The main change feature is that bone resorption of the superior orbital rim is more obvious than that of the inferior orbital rim in the aging process, which verifies the view of Pessa and Chen.¹⁶

Additionally, in this research, the overall shape features (area, height, perimeter, and circularity of the connected component) of orbit contours were extracted with the connected component shape description algorithm, finding that the area and height values of orbits of 3 age groups were not distributed regularly. This result supports the theory of Jeon,¹⁸ but is contrary to the view of Kahn¹⁵ and Ching.¹⁷ There may be 2 reasons. First, the data size of the literatures^{15,17,18} and this paper is not large enough. Second, both the experiment object of this paper and the experiment object (South Korean) in literature¹⁸ are Mongolian. For the perimeter, circularity and other features of the connected component of orbits among groups at different ages, no differential results of statistical significance were obtained. On the whole, changes of several simple overall contour shape features were not obvious in the process of aging, such as area and height, that is, the association between simple overall features and the aging degree is very weak.

At last, identification was validated with the shape context algorithm. When the shape was described with the shape context method, the weight of all the subareas was totally the same. With CNN, the weight of partial features which made more contributions to the identification result was improved through training. Additionally, with CNN featured with combination of convolution and pooling, complex shape features composed of the basic point and line features of images were extracted. The identification accuracy of CNN is much larger than that of the shape context, which reflects that the aging features are mainly in partial areas of the orbit contour, and the feature type is the partial shape change. This further proves that as people get older, the aging change of the middle part of the superior orbital rim of Mongolian bony orbits is more obvious than that of inferior orbital rim.

CONCLUSIONS

This paper puts forward a method for automatic segmentation of bony orbit contour as well as automatic extraction and classification of orbit aging features based on the segmentation result. U-Net can

realize high-precision segmentation of the orbit contour, and with the CNN-based orbit contour sorting algorithm, the aging degree of the bony orbit can be identified precisely. It is preliminarily validated that the aging mode of Mongolian bony orbit contour is that the bone resorption of the superior orbital rim is more obvious than that of the inferior orbital rim, and the change of the orbit area, perimeter, height and circularity is not obvious in the aging process. In our future work, we will collect more data, validate such data with the method put forward in this article, and quantize changes of aging features of orbit contours with automatic methods.

REFERENCES

- Lambros V. Observations on periorbital and midface aging. *Plast Reconstr Surg* 2007;120:1367–1376
- Varani J, Spearman D, Perone P, et al. Inhibition of type I procollagen synthesis by damaged collagen in photoaged skin and by collagenase-degraded collagen in vitro. *Am J Pathol* 2001;158:931–942
- Gosain AK, Klein MH, Sudhakar PV, et al. A volumetric analysis of soft-tissue changes in the aging midface using high-resolution MRI: implications for facial rejuvenation. *Plast Reconstr Surg* 2005;115:1143–1152
- Farkas JP, Pessa JE, Hubbard B, et al. The science and theory behind facial aging. *Plast Reconstr Surg Glob Open* 2013;1:8–15
- Matros E, Momoh A, Yaremchuk MJ. The aging midfacial skeleton: implications for rejuvenation and reconstruction using implants. *Facial Plast Surg* 2009;25:252–259
- Shaw JRB, Katzel EB, Koltz PF, et al. Facial bone density: effects of aging and impact on facial rejuvenation. *Aesthet Surg J* 2012;32:937–942
- Wong C, Mendelson B. Newer understanding of specific anatomic targets in the aging face as applied to injectables: aging changes in the craniofacial skeleton and facial ligaments. *Plast Reconstr Surg* 2015;136:44S–48S
- Pessa JE. An algorithm of facial aging: verification of Lambros's theory by three-dimensional stereolithography, with reference to the pathogenesis of midfacial aging, scleral show, and the lateral suborbital trough deformity. *Plast Reconstr Surg* 2000;106:479–488
- Mendelson BC, Hartley W, Scott M, et al. Age-related changes of the orbit and midcheek and the implications for facial rejuvenation. *Aesthet Plast Surg* 2007;31:419–423
- Shaw RB, Kahn DM. Aging of the midface bony elements: a three-dimensional computed tomographic study. *Plast Reconstr Surg* 2007;119:675–681
- Jeon A, Sung KH, Kim SD, et al. Anatomical changes in the East Asian midface skeleton with aging. *Folia Morphol (Warsz)* 2017;76:730–735
- Escaravage GK, Dutton JJ. Age-related changes in the pediatric human orbit on CT. *Ophthalmic Plast Reconstr Surg* 2013;29:150–156
- Toledo AL, Cardoso MA, Santos BL, et al. Aging and sexual differences of the human skull. *Plast Reconstr Surg Glob Open* 2017;5:e1297
- Kim J, Park SW, Choi J, et al. Ageing of the bony orbit is a major cause of age-related intraorbital fat herniation. *J Plast Reconstr Aesthet Surg* 2018;71:658–664
- Kahn D, Shawjr R. Aging of the bony orbit: a three-dimensional computed tomographic study. *Aesthet Surg J* 2008;28:258–264
- Pessa JE, Chen Y. Curve analysis of the aging orbital aperture. *Plast Reconstr Surg* 2002;109:751–755
- Ching JA, Ford JM, Decker SJ. Aging of the adult bony orbit. *J Craniofac Surg* 2020;31:1082–1085
- Jeon A, Lee U, Kwak D, et al. Aging of the bony orbit in East Asians: a three-dimensional computed tomographic study. *Surg Radiol Anat* 2020;42:617–626
- Wang S, Kang B, Ma J, et al. A deep learning algorithm using CT images to screen for Corona virus disease (COVID-19). *Eur Radiol* 2021;31:6096–6104
- Tan X, Li K, Zhang J, et al. Automatic model for cervical cancer screening based on convolutional neural network: a retrospective, multicohort, multicenter study. *Cancer Cell Int* 2021;21:35
- Li L, Song X, Guo Y, et al. Deep convolutional neural networks for automatic detection of orbital blowout fractures. *J Craniofac Surg* 2020;31:400–403
- Ronneberger O, Fischer P, Brox TU. U-Net: Convolutional Networks for Biomedical Image Segmentation. International Conference on Medical Image Computing and Computer-Assisted Intervention 2015:234–241
- Byra M, Jarosik P, Szubert A, et al. Breast mass segmentation in ultrasound with selective kernel U-Net convolutional neural network. *Biomed Signal Process Control* 2020;61:102027
- Long J, Ma G, Liu H, et al. Cascaded hybrid residual U-Net for glioma segmentation. *Multimed Tools Appl* 2020;79:24929–24947
- Long F. Microscopy cell nuclei segmentation with enhanced U-Net. *BMC Bioinform* 2020;21
- Pessa JE. The potential role of stereolithography in the study of facial aging. *Am J Orthod Dentofacial Orthop* 2001;119:117–120
- Krizhevsky A, Sutskever I, Hinton GE. ImageNet classification with deep convolutional neural networks. *Adv Neural Inf Process Syst* 2012;25:1097–1105
- Srivastava N, Hinton G, Krizhevsky A, et al. Dropout: a simple way to prevent neural networks from overfitting. *J Mach Learn Res* 2014;15:1929–1958
- Belongie S, Malik J, Puzicha J. Shape matching and object recognition using shape contexts. *IEEE Trans Pattern Anal Mach Intell* 2002;24:509–522
- Greg M, Serge B, Jitendra M. Efficient shape matching using shape contexts. *IEEE Trans Pattern Anal Mach Intell* 2005;27:1832–1837
- Kingma DP, Ba J. Adam: A method for stochastic optimization. 3rd International Conference on Learning Representations 2015:1–13
- Cover T, Hart P. Nearest neighbor pattern classification. *IEEE Trans Inform Theory* 1967;13:21–27
- Fushiki T. Estimation of prediction error by using K-fold cross-validation. *Stat Comput* 2011;21:137–146